APPENDIX D

ANALYTICAL EXPRESSIONS INCORPORATING RESTRAINT OF PRESSURE-INDUCED BENDING IN CRACK-OPENING DISPLACEMENT CALCULATIONS

D. 1 Introduction

Among the factors that are important to leak-before-break (LBB) of nuclear piping systems is an effect called restraint of pressure-induced bending on crack-opening displacement (Ref. D.1). As shown in Figure D.1, the existence of a through-wall circumferential crack will result in a bending moment at the crack region for a pipe loaded axially from pressure, due to the eccentricity from the neutral axis in the cracked plane versus the center of the uncracked pipe. This pressure-induced bending (PIB) causes an unrestrained pipe to rotate, thereby resulting in an increase in crack-opening displacement.

In a real piping system, the ends of the pipe can be restrained from free rotation, reducing the degree of pressure-induced bending. Examples of the pipe restraints include nozzles, elbows, pipe hangers, and other pipe-system boundary conditions. The degree of the restraint also depends on the geometry of the pipe system. In general, the restraint of end rotation is a function of:

- the magnitude of the load (elastic or plastic effects),
- the length of the crack,
- the pipe geometry, i.e., R/t ratio, and
- the boundary conditions of the pipe on either side of the crack location.

The restraining effect on PIB in general results in an increase in the load-carrying capacity of the cracked pipe, but a decrease in the crack-opening displacement when compared with that of the same cracked pipe free from the restraints (Ref. D.2). This is illustrated in Figure D.2.

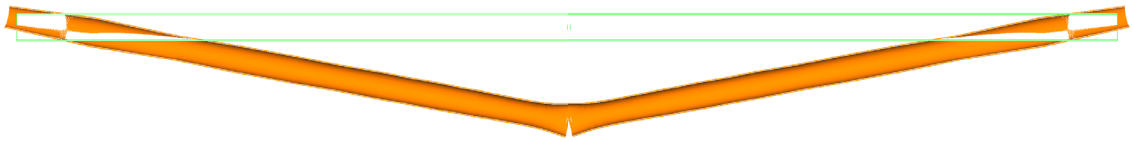

Figure D.1 Rotation of unrestraint pipe due to pressure induced bending. The rotation of the pipe is magnified by factor of 2.

Figure D.2 Reduction of COD in pressure-induced-bending of a restrained pipe. An asymmetric pipe restraint condition is shown. Displacement magnified by a factor of 5.

The beneficial load-carrying capacity increase has a corresponding decrease in the cracking-opening area for leak detection that is detrimental to LBB. The trade-offs between the two effects appear to be case-dependent, and are influenced by the pipe diameter and crack length (Ref. D.3).

The common analysis practice for LBB is to determine the center crack-opening displacement (COD) by using the solution for an end-capped vessel. The so-called end-capped vessel model, although relatively simple to analyze, allows the ends of the vessel to freely rotate. Furthermore, it ignores the restraint to the ovalization at the crack plane imposed by the restraining end of the piping system. Therefore, the end-capped vessel model may over-estimate the COD more than if the pipe is not allowed to rotate in the real world piping systems.

In this program, a set of analytically based expressions has been developed. These expressions can be used to correct the end-capped COD solutions to account for the effect of piping restraint on PIB. The expressions are given in terms of the normalizing factor r_{COD}, defined as:

$$r_{COD} = \frac{COD_{res}}{COD_{unres}} \qquad (D.1)$$

where COD_{res} is the COD value of a crack in a restrained piping system, and COD_{unres} is the COD value in the corresponding unrestrained pipe. r_{COD} is also called the normalized COD. Solutions for COD_{unres} for various pipe and crack geometries are available in many publications in open literature. They can also be obtained rather easily using the end-capped vessel models. Once the COD_{unres} is known, the COD of a crack in a restrained pipe can be determined with the aid of the normalizing factor r_{COD} derived in this work:

$$COD_{res} = r_{COD} \cdot COD_{unres} \qquad (D.2)$$

The analytical expressions obtained in this work were based the results of the round-robin finite element (FE) calculations of COD values that were conducted earlier in this BINP program (Ref. D.4). As such, the expressions of the normalizing factor are limited, and should be used within the range in which the expressions were derived.

D. 2 Problem Statement

Due to the bending and the rotation of a cracked pipe, the crack-opening displacement is not uniform through the wall of the pipe – the crack-opening displacement at the inner surface of the pipe can be different from that at the outer surface. In this program, the term COD is specifically referred to as the *center crack opening displacement at the mid-thickness* of a through-wall circumferential crack in a straight pipe.

The cracked-pipe geometry investigated in this program is illustrated in Figure D.3. The basic geometric variables include the pipe outside diameter (OD), pipe mean radius to thickness ratio (R_m/t), half crack length (θ), and the restraint length – the distance between the restraint plane and the crack plane (L_{R1}, L_{R2}). The restraint is called symmetric if the restraint lengths from both ends are equal ($L_{R1}=L_{R2}=L_R$); otherwise, it is called asymmetric restraint. These variables are also given in Figure D.3.

The basic assumptions made in both the round-robin FE analyses and the derivation of the analytical expressions are:

- The deformation is linear elastic. The elastic modulus is 200 GPa (29,000 ksi), and the Poisson's ratio is 0.3.
- The displacement of the pipe is small – both the strain and the rotation of a cracked pipe from PIB are small. As such, the geometric nonlinearity effects due to large rotation and large strain are ignored. Also ignored is the change of loading directions associated with the deformation process.
- At the crack plane, the pipe is allowed to move vertically and horizontally (rotation in the crack plane and ovalization are not restricted), but it was pinned of any axial displacement in the ligament.
- For the restrained pipe, both ends of the pipe are restrained from rotation and ovalization, and only the axial displacement is allowed at the pipe end. This represents the most severe restraint conditions in a piping system.
- For the reference unrestrained pipe, the end-capped vessel model is assumed – the ends of the pipe are allowed to move freely. Theoretically, the unrestrained pipe should be infinitely long. The results from the round-robin FE calculations show that, if the pipe length is greater than 20 times of the pipe diameter ($L_R > 20$ OD), the pipe ends will then have negligible effect on the deformation in the vicinity of the cracked plane and the resultant COD value.
- An axial force is applied at the pipe end, passing through the central axis of the pipe. The applied load values are arbitrarily chosen because; (1) the deformation is

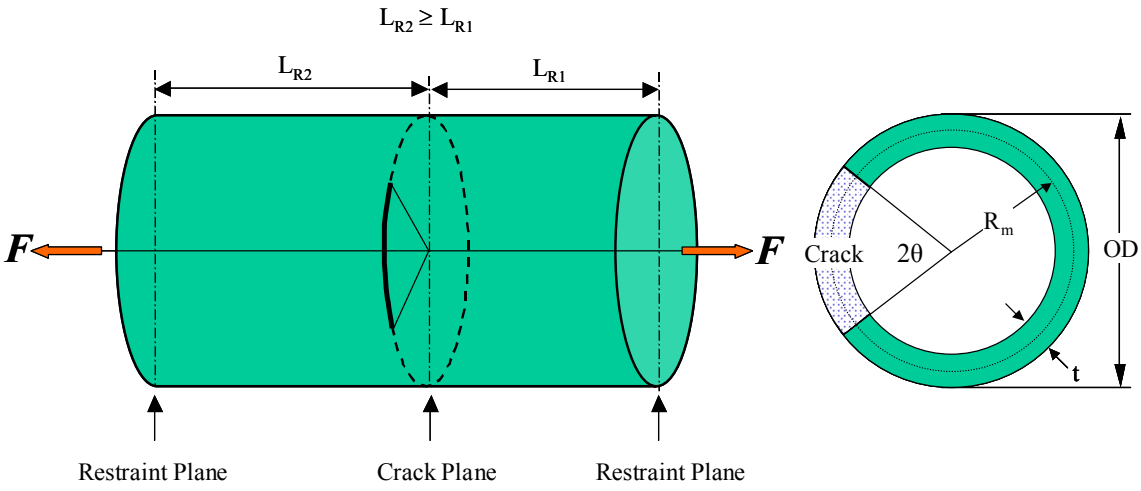

Figure D.3 Cracked-pipe geometry

linear-elastic and confined to the small displacement condition, and (2) the COD results are normalized with respect to the unrestrained COD.

- There is no pressure on the crack faces, and no internal pressure is present.

Figure D.4 depicts the boundary and loading conditions used in this investigation for the symmetrically restrained cases (L_1=L_2).

D.2.1 Round-Robin FE COD Analyses

The BINP round-robin FE COD analysis matrix included a total of 144 cases covering a wide range of pipe geometries and restraint conditions (Ref. D.4). Table D.1 and Table D.2 summarize the analysis matrix of the round-robin FE calculations. Details of the round-robin analysis can be found in Reference D.4. The results from the round-robin analysis were used to validate the analytical expressions developed in this work.

D.3 Development of Analytical Expressions

The development of the analytical expressions for restraint of pressure induced bending was based on the recent work by Miura (Ref. D.5). Miura's expression was expanded to cover a wider range of R/t ratios for a symmetrically restrained pipe system. New expressions were developed for the asymmetric restraint conditions.

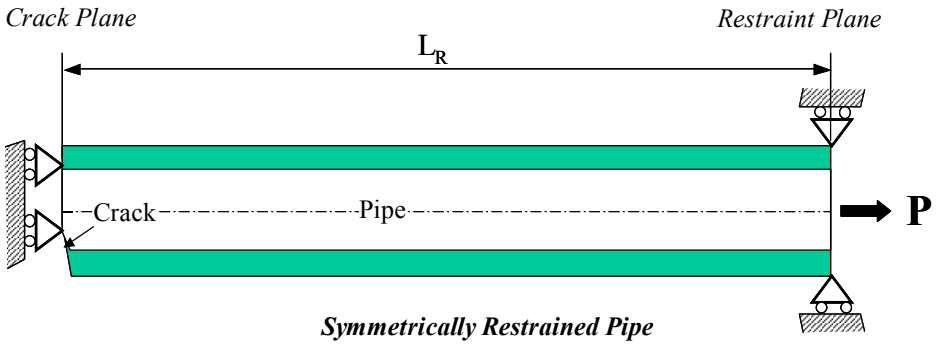

Symmetrically Restrained Pipe

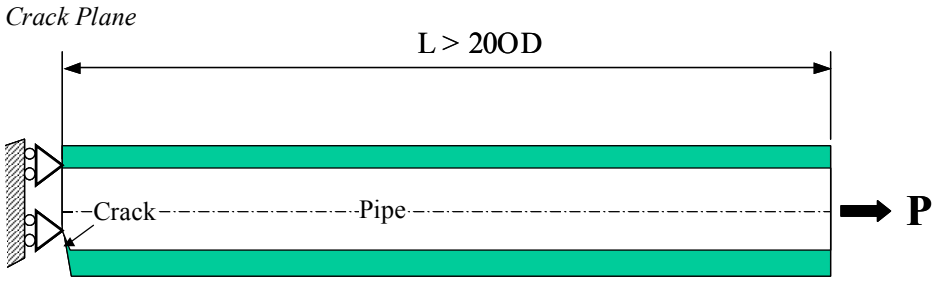

Unrestrained Pipe

Figure D.4 Loading and boundary conditions of a symmetrically restrained pipe

Table D.1 Analysis matrix for symmetric restraint cases in round-robin FE calculations

	OD (mm)	R_m/t	Axial Force (kN)	Half Crack Length			Restraint Length (L/OD)			
Case 1a	711.2	10	50,000	π/8	π/4	π/2	1	5	10	20
Case 1b	323.85	10	5,000	π/8	π/4	π/2	1	5	10	20
Case 1c	114.3	10	500	π/8	π/4	π/2	1	5	10	20
Case 2a	711.2	5	50,000	π/8	π/4	π/2	1	5	10	20
Case 2b	711.2	20	50,000	π/8	π/4	π/2	1	5	10	20
Case 2c	711.2	40	50,000	π/8	π/4	π/2	1	5	10	20

Table D.2 Analysis matrix for asymmetric restraint cases in round-robin FE calculations

	OD (mm)	Rm/t	Axial Force (kN)	Half Crack Length			L_{R_2}/OD			L_{R_1}/OD
							5	**10**	**20**	
Case 3a	711.2	10	50,000	π/8	π/4	π/2	X	X	X	1
	711.2	10	50,000	π/8	π/4	π/2		X	X	5
	711.2	10	50,000	π/8	π/4	π/2			X	10
Case 3b	323.85	10	5,000	π/8	π/4	π/2	X	X	X	1
	323.85	10	5,000	π/8	π/4	π/2		X	X	5
	323.85	10	5,000	π/8	π/4	π/2			X	10
Case 3c	114.3	10	500	π/8	π/4	π/2	X	X	X	1
	114.3	10	500	π/8	π/4	π/2		X	X	5
	114.3	10	500	π/8	π/4	π/2			X	10

D.3.1 Symmetrically Restrained Pipe

Miura's approach is schematically illustrated in Figure D.5. Miura treated the deflection of a cracked pipe due to pressure-induced bending as an elastic beam problem. The existence of the crack is represented by a beam section of reduced thickness in the vicinity of the cracked plane. The end-restraint of the pipe makes the deflection of the beam statistically indeterminate. He then makes the analogy that the COD and pipe rotations are linearly related, hence the ratios of the restrained to the unrestrained rotation is the same as the ratio for the restrained to unrestrained COD. Such an approach has also been used for developing J-estimation schemes in the past.

For symmetric restraint, Miura derived the following equation for the normalizing factor (normalized COD), r_{COD}:

$$r_{COD} = \frac{L_R / D_m}{L_R / D_m + \dfrac{I_b(\theta)}{4}} \qquad (D.3)$$

where D_m is the mean diameter of the pipe, L_R the restraint length, and θ the half-crack angle. $I_b(\theta, R_m/t)$ is an integral of the compliance term, $F_b(\theta, R_m/t)$, in the stress intensity factor definition, K_I:

$$I_b(\theta, R_m/t) = 4\int \theta \, F_b^2(\theta, R_m/t)\, d\theta$$
$$K_I = \sigma_b \sqrt{\pi R_m \theta}\; F_b(\theta, R_m/t) \qquad (D.4)$$

According to Equation D.3, r_{COD} is related to the normalized geometric parameters:

- normalized restraint length L_R/D_m,
- normalized pipe thickness R_m/t, and
- normalized half crack length θ/π.

Such a parametric relationship simplifies the application of the analytical expressions – it is unnecessary to distinguish the results from pipes with different diameters or restraint lengths, provided that the normalized parameters are the same. Indeed, the results from the round-robin FE calculations, as illustrated in Figure D.6, support the parametric relationship.

Miura used the following equations to evaluate the function $I_b(\theta, R_m/t)$:

$$I_b(\theta, R_m/t) = 2\theta^2\left[1 + 8\left(\frac{\theta}{\pi}\right)^{1.5} I_{b1} + \left(\frac{\theta}{\pi}\right)^3 (I_{b2} + I_{b3})\right]$$
$$I_{b1} = \frac{A_b}{7} + \frac{B_b}{9}\left(\frac{\theta}{\pi}\right) + \frac{C_b}{11}\left(\frac{\theta}{\pi}\right)^2 \qquad (D.5)$$
$$I_{b2} = \frac{A_b^2}{2.5} + \frac{A_b B_b}{1.5}\left(\frac{\theta}{\pi}\right) + \frac{2A_bC_b + B_b^2}{3.5}\left(\frac{\theta}{\pi}\right)^2$$
$$I_{b3} = \frac{B_bC_b}{2}\left(\frac{\theta}{\pi}\right)^3 + \frac{C_b^2}{4.5}\left(\frac{\theta}{\pi}\right)^4$$

where the coefficients A_b, B_b, and C_b are taken from Klecker et al.'s curve-fitting of Sander's solution for the stress intensity factor (Ref. D.6). These original coefficient are given in Equation D.6.

In this study, it was found that the coefficients used by Miura, as given in Equation D.6, are only valid for R_m/t ratios up to 16. Thus, these coefficients were revised to cover a wider range of R_m/t ratios up to 40, again through curve-fitting the Sander's solution. The revised coefficients are given in Equation D.7.

The differences in $I_b(\theta, R_m/t)$ are compared in Figure D.7. Clearly the discrepancies are significant for R_m/t values above 20.

Figures D.8 though Figure D.11 provide comparisons of the r_{COD} from the analytical expressions and the FE calculations for all the symmetric restraint cases in the round-robin analysis matrix. The analytical solutions are shown as solid lines, whereas the FE results are shown as various points in these figures. Clearly, the analytical expression by Miura (Equation D.3), combined with the revised coefficients (Equation D.7), is adequate for all the cases investigated in the present study. For comparison, Figure D.12 shows the analytical solution using the original coefficients by Miura for $R_m/t = 40$. The use of the original coefficients severely underestimates the values of r_{COD}, especially for the cases where the crack is long.

$$\begin{bmatrix} A_b \\ B_b \\ C_b \end{bmatrix} = \begin{bmatrix} -3.26543 & 1.52784 & -0.072698 & 0.0016011 \\ 11.36322 & -3.91412 & 0.18619 & -0.004099 \\ -3.18609 & 3.84763 & -0.18304 & 0.00403 \end{bmatrix} \begin{bmatrix} 1 \\ R_m/t \\ (R_m/t)^2 \\ (R_m/t)^3 \end{bmatrix} \qquad \text{for } R_m/t < 16 \quad (D.6)$$

$$\begin{bmatrix} A_b \\ B_b \\ C_b \end{bmatrix} = \begin{bmatrix} -2.6925 & 1.3148 & -0.049146 & 0.00080685 \\ 9.7042 & -3.3423 & 0.12768 & -0.0021944 \\ -1.9277 & 3.3798 & -0.13131 & 0.0022859 \end{bmatrix} \begin{bmatrix} 1 \\ R_m/t \\ (R_m/t)^2 \\ (R_m/t)^3 \end{bmatrix} \qquad \text{for } R_m/t < 40 \quad (D.7)$$

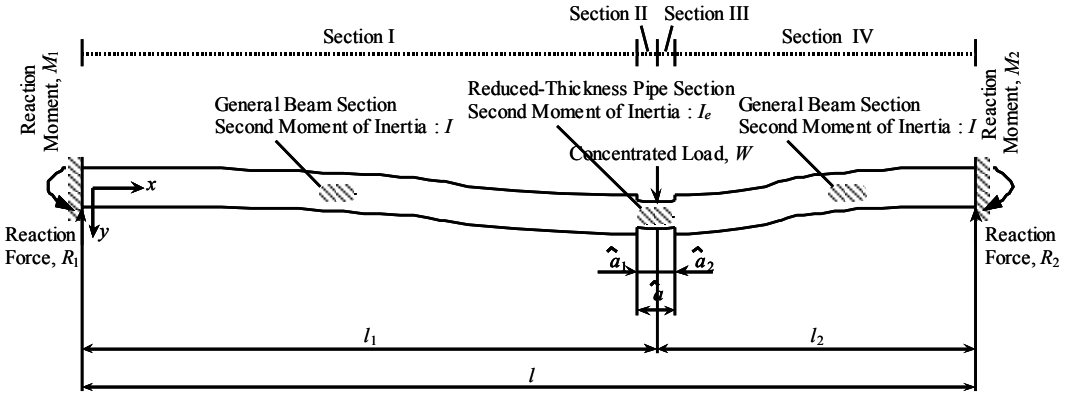

Figure D.5 Beam model representing deformation of cracked pipe under restraint (Ref. D.5)

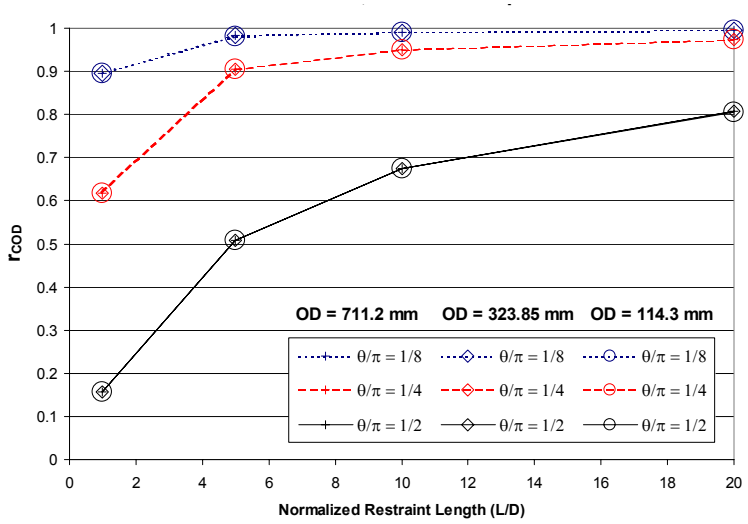

Figure D.6 Normalized COD for different pipe diameters (Ref. D.4)

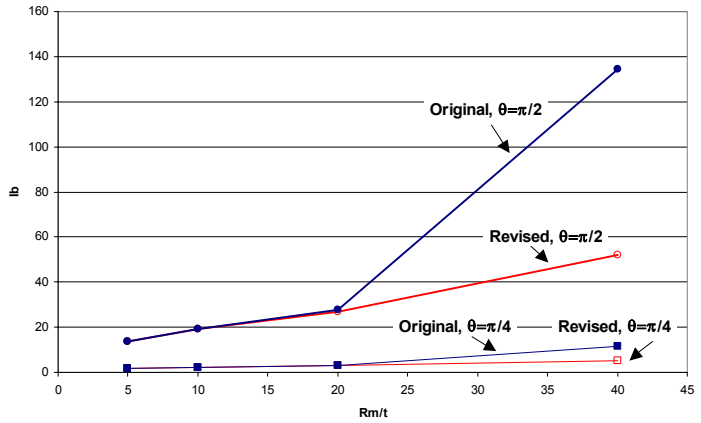

Figure D.7 Comparison of the $I_b(\theta)$ values for different curve-fitting coefficients

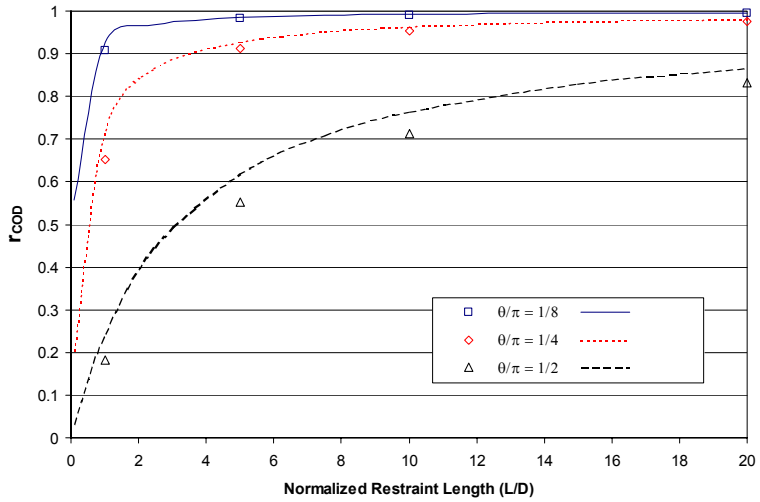

Figure D.8 Comparison of the normalizing factor between the analytical expression and the FE calculations. Symmetric restraint, $R_m/t=5$

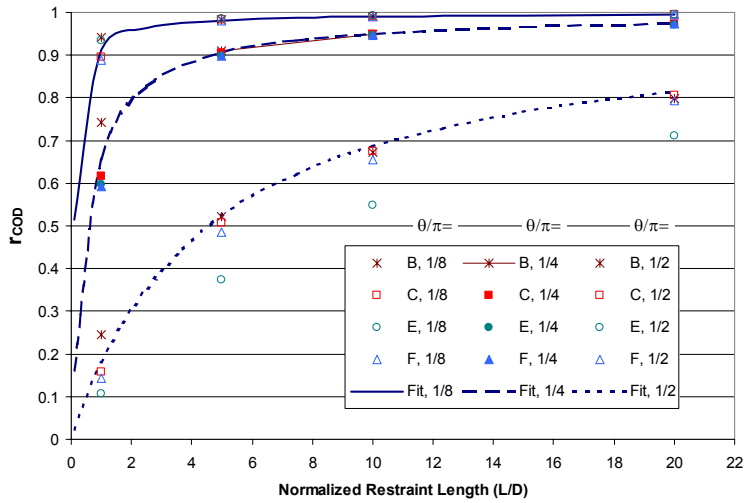

Figure D.9 Comparison of the normalizing factor between the analytical expression and the FE calculations. The FE results from different round-robin participants are indicated by different letters. Symmetric restraint, $R_m/t=10$

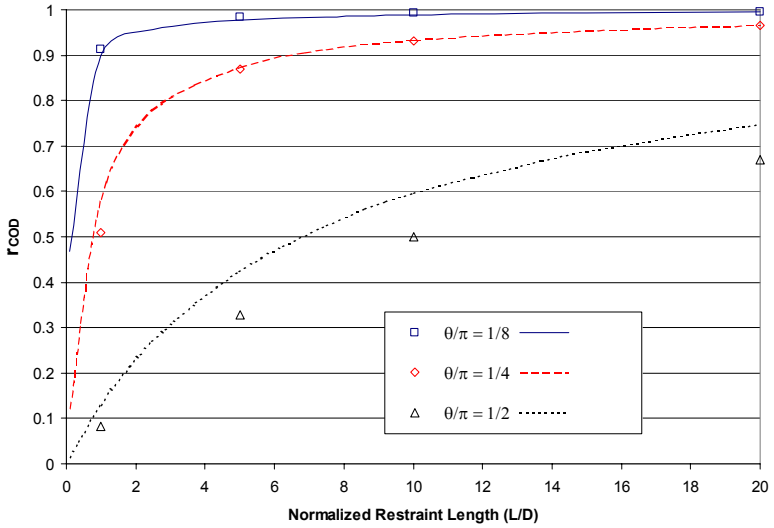

Figure D.10 Comparison of the normalizing factor between the analytical expression and the FE calculations. Symmetric restraint, $R_m/t=20$

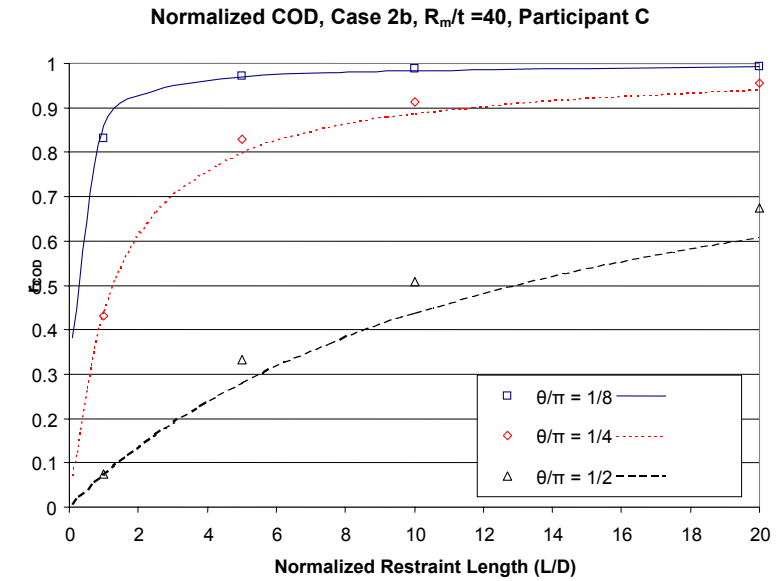

Figure D.11 Comparison of the normalizing factor between analytical expression and the FE calculations. Symmetric restraint, $R_m/t=40$

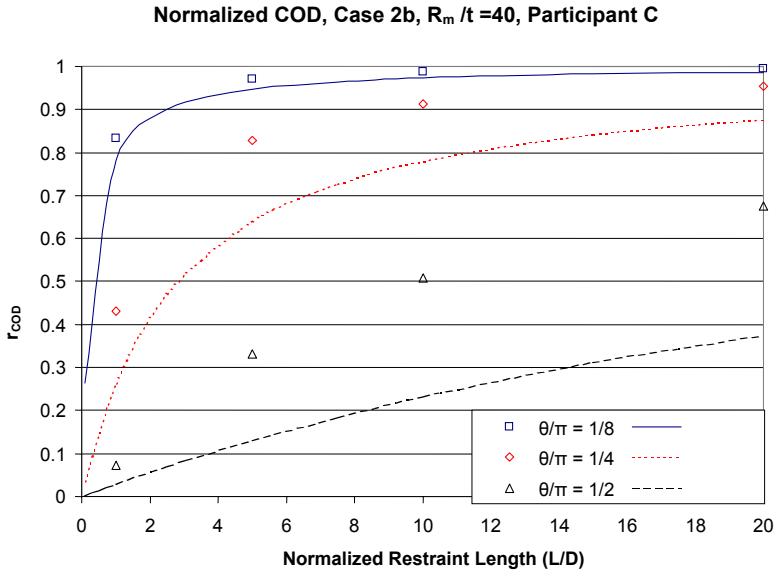

Figure D.12 Comparison of the normalizing factor between the analytical expression and the FE calculations. Symmetric restraint, $R_m/t=40$. NUREG/CR-4572 curve-fitting of coefficients of A_b, B_b, and C_b

D.3.2 Asymmetrically Restrained Pipe

Using the same beam approach for the symmetric restraint case, Miura derived the following solution for the asymmetrical restraint case:

$$r_{COD} = \frac{[L_R/D_m]_{eq}}{[L_R/D_m]_{eq} + \frac{I_b(\theta)}{4}} \qquad (D.8)$$

where $[L_R/D_m]_{eq}$ is the so-called equivalent normalized restraint length:

$$[L_R/D_m]_{eq} = 2\frac{[L_{R1}/D_m][L_{R2}/D_m]}{[L_{R1}/D_m]+[L_{R2}/D_m]} \quad or \quad \frac{1}{[L_R/D_m]_{eq}} = \frac{1}{2}\left(\frac{1}{[L_{R1}/D_m]} + \frac{1}{[L_{R2}/D_m]}\right) \qquad (D.9)$$

As shown in Equation D.9, the equivalent normalized restraint length is the harmonic average of the normalized restraint lengths L_{R1} and L_{R2}.

Comparisons with the round-robin FE results reveals that the Miura's solution tends to underestimate the restraint effect if the restraint length is short, and overestimate if the restraint length is long. The discrepancy is especially noticeable if the crack is long and the asymmetry of the restraint length is large, as shown in Figure D.13.

It appears that the inadequacy of Miura's solution for the asymmetric cases is related to the harmonic property of the equivalent normalized restraint length. To illustrate this point, rearranging Equation D.9 yields:

$$[L_R/D_m]_{eq} = 2\frac{[L_{R1}/D_m][L_{R2}/D_m]}{[L_{R1}/D_m]+[L_{R2}/D_m]} = 2\frac{L_{R1}/D_m}{1+L_{R1}/L_{R2}} \qquad (D.10)$$

If L_{R2} is the longer restraint length of the two, then

$$L_{R1}/L_{R2} < 1 \quad and \quad [L_R/D_m]_{eq} < 2L_{R1}/D_m \qquad (D.11)$$

This means that, regardless the length of the longer restraint L_{R2}, the harmonic equivalent normalized restraint length cannot be greater than twice of the shorter restraint length. The variation of the harmonic equivalent restraint length as function of the L_{R2}/L_{R1} is shown in Figure D.14.

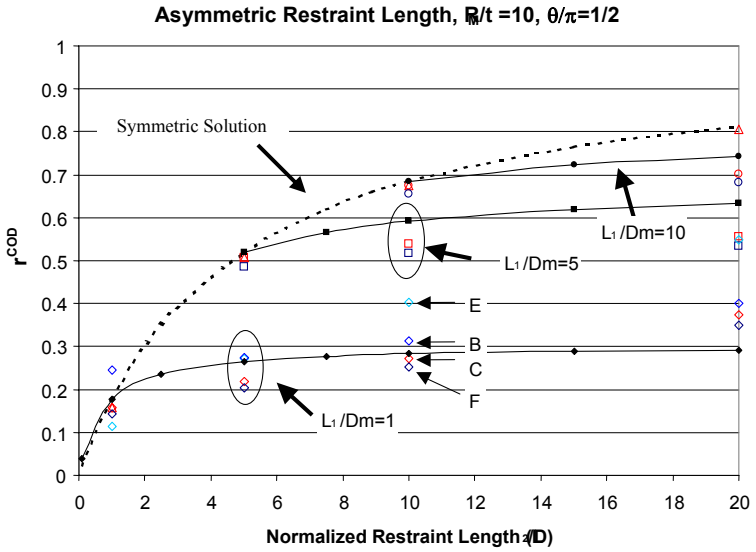

Figure D.13 Comparison of Miura's analytical solution with FE results for asymmetric restraint cases. Letters indicate the FE results from different round-robin participants. $R_m/t=10$, $\theta=\pi/2$

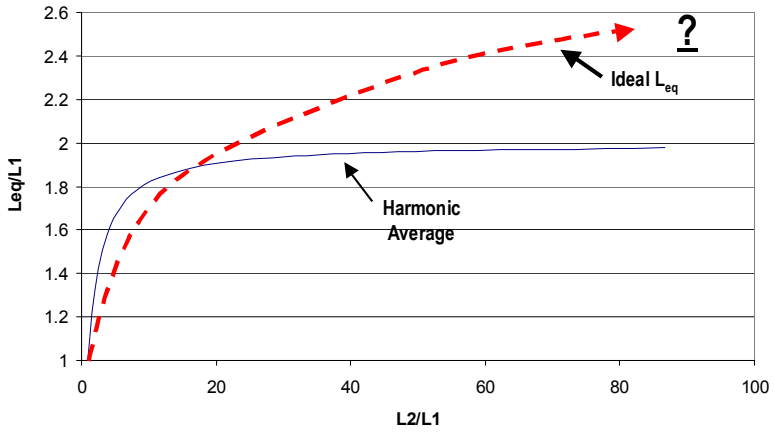

Figure D.14 Equivalent normalized restraint length as function of the ratio of L_{R2}/L_{R1}

Now consider a special case in which a pipe is restrained only at one end, at a distance of one D_m from the crack plane (i.e., $L_{R1}/D_m = 1$ and $L_{R2} \to \infty$). Equation D.10 becomes:

$$[L_R / D_m]_{eq} = \frac{2[L_{R2} / D_m]}{1 + [L_{R2} / D_m]} = \frac{2}{1 + \frac{1}{[L_{R2} / D_m]}} = 2 \qquad (D.12)$$

Hence, the harmonic equivalent normalized restraint length can only reach 2 even if the pipe is restrained only at one end. Further assuming $R_m/t=10$ and $\theta=\pi/2$, the resultant r_{COD} is 0.286, as shown in Figure D.13.

The same case was also analyzed using FE approach. The model is shown in Figure D.15. The restraint boundary condition was applied at $L_{R1}/D_m = 1$ from the crack plane at the left end of the pipe. The length of the pipe on the right side of the crack was set at $20D_m$, but the end was left unrestrained to allow free rotation and ovalization (end-capped condition). This effectively represents an infinitely long restraint length at the right side of the crack ($L_{R2}/D_m \to \infty$).

The r_{COD} from the FE model is 0.93, more than three times higher than the value obtained with the harmonic equivalent restraint length. Clearly, the harmonic expression of the equivalent restraint length penalizes the contribution of the longer pipe restraint length, and thus is inadequate if the restraint length of the longer pipe is relatively long.

More importantly, the FE analysis suggests that the restraint effect is nearly negligible ($r_{COD} \to 1$) in a one-side restrained pipe. This means that

$$L_{eq} \to \infty \quad if \; L_{R1} \neq 0 \; and \; L_{R2} \to \infty \qquad (D.13)$$

Therefore, an improved definition of L_{eq} is required to improve the accuracy of the analytical expression of r_{COD} for the asymmetric restraint conditions. However, derivation of a theoretically sound closed-form analytic L_{eq} definition was found to be difficult.

A different approach was then adopted in this work – a correction function was used to relate the solution for asymmetrically restrained pipe to symmetrically restrained pipe. The correction function is proposed to take the following form:

$$r_{COD,asym} = (r_{COD,sym})_{L_{R1}} + \left[1 - (r_{COD,sym})_{L_{R1}}\right] \cdot \min\left(\frac{\ln(L_{R2}/L_{R1})}{\ln(L_{ref}/L_{R1})}, 1\right) \qquad for \; L_{R1} < L_{R2} \qquad (D.14)$$

where $r_{COD,\ asym}$ is the normalizing factor for the asymmetrically restrained pipe. $(r_{COD,\ sym})_{LR1}$ is for the corresponding symmetrically restrained pipe, evaluated using Equation D.3 with the shorter restraint length L_{R1}. L_{ref} is a reference restraint length, representing the restraint length above when the restraint effect is negligible.

The correction function is expected to take the shape as illustrated in Figure D.16, and has the following properties:

$$r_{COD,\ asym} = r_{COD,\ sym} \quad if\ L_{R2} = L_{R1}$$
$$and \qquad (D.15)$$
$$r_{COD} \to 1 \quad if\ L_{R2} \to L_{ref}$$

L_{ref} is the only unknown variable of the correction function. L_{ref} is expected to be a function of R/t ratio and half crack length. Its values can be determined through curve-fitting of the FE calculation results. In this work, curve-fitting the round-robin FE calculations results in the second-order polynomial equation for L_{ref}, given in Equation D.16. The equation is plotted in Figure D.17.

The correction function for the asymmetrically restrained pipe is validated using the round-robin FE results. They are shown in Figrue D.18 to Figure D.20. Miura's solutions for the asymmetric case with the harmonic equivalent restraint length are also shown in the figures for comparison. The correction function clearly improves the accuracy of the analytical expressions of the normalizing factor.

$$\ln(L_{ref}/L_{R1}) = 38.52713\left(\frac{\theta}{\pi}\right)^2 - 5.658775\left(\frac{\theta}{\pi}\right) + 4.710531 \quad for \quad R_m/t = 10 \text{ and } \frac{1}{8} < \frac{\theta}{\pi} < \frac{1}{2} \qquad (D.16)$$

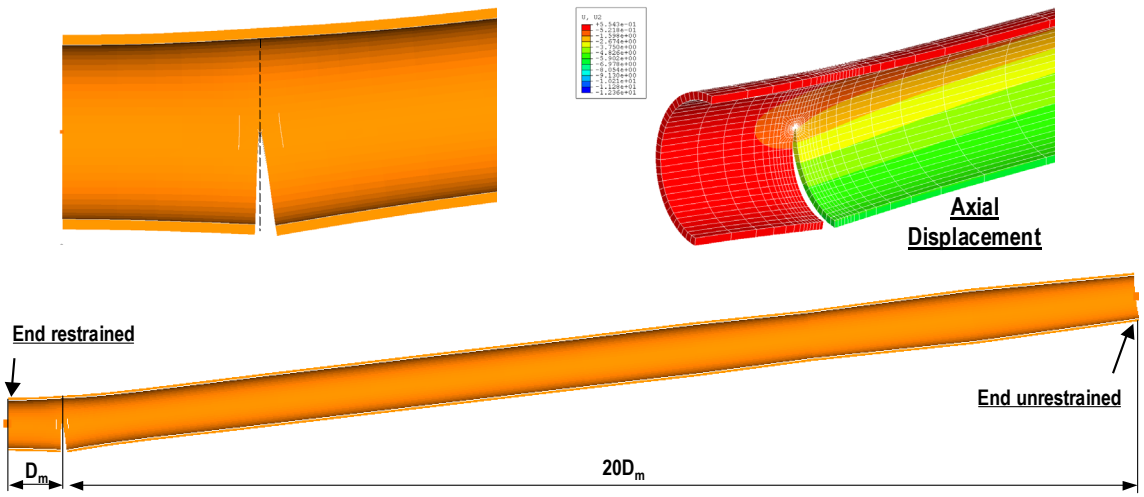

Figure D.15 PIB of a cracked pipe with one-sided restraint. $\theta=\pi/2$, $R_m/t=10$, $L_{R1}/D_m=1$, $L_{R2}/D_m\to\infty$

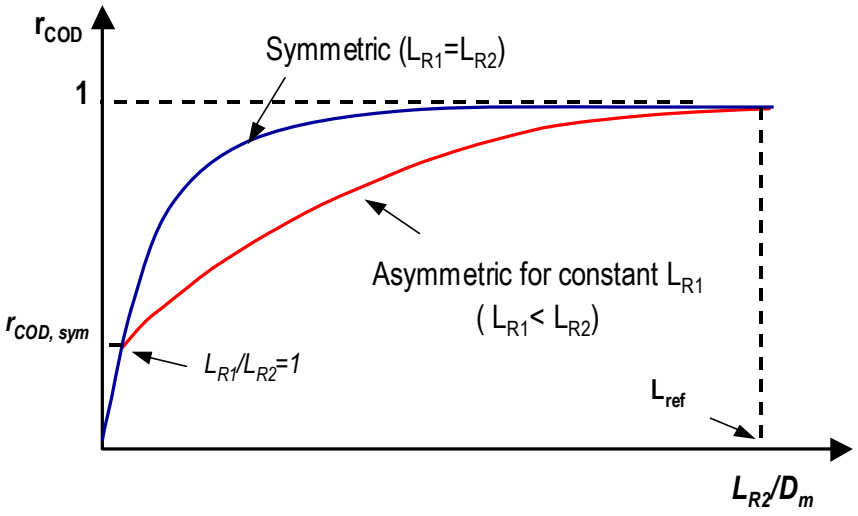

Figure D.16 General form of the correction function

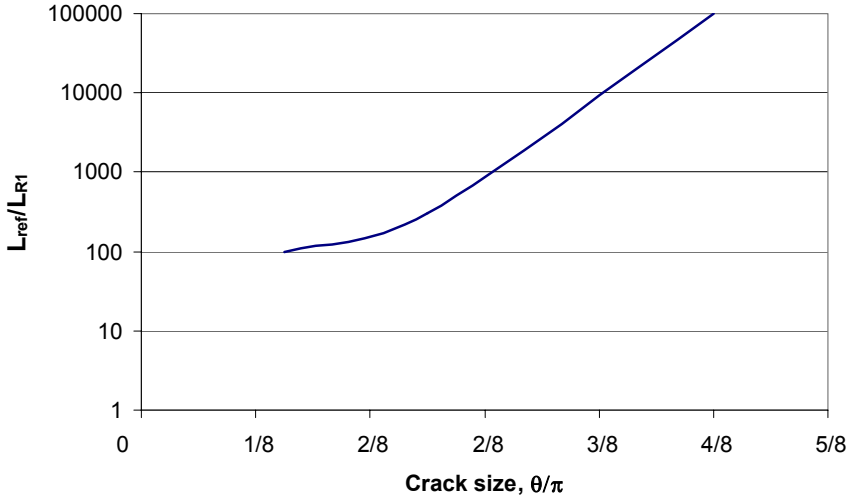

Figure D.17 Reference restraint length as function of crack size (R_m/t=10)

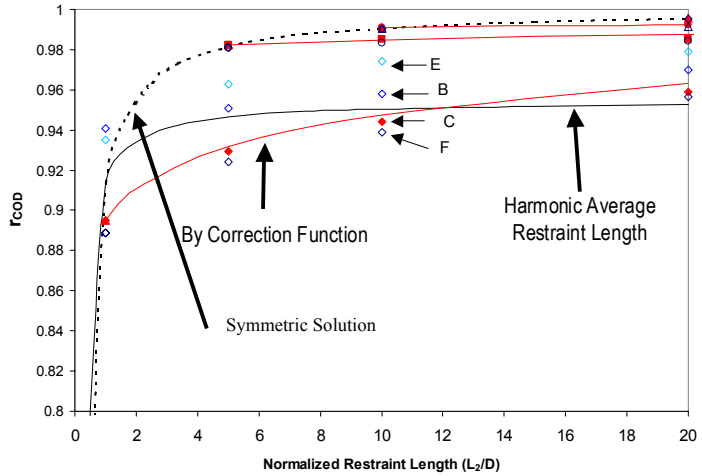

Figure D.18 Verification of analytical expression for asymmetric restraint cases (R_m/t=10, θ=π/8)

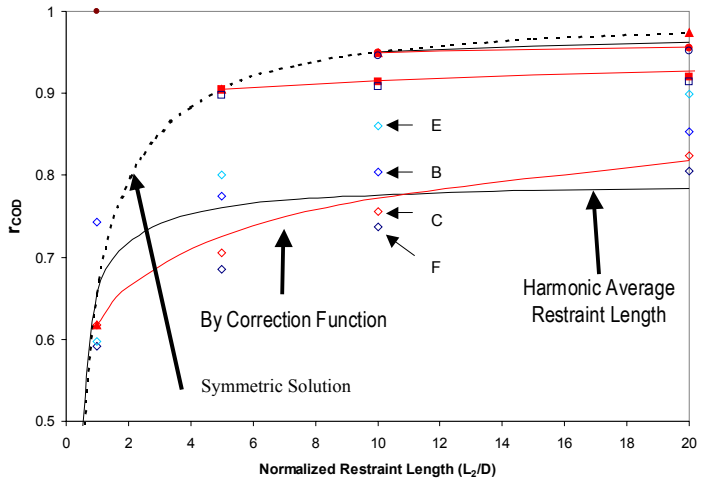

Figure D.19 Verification of analytical expression for asymmetric restraint cases ($R_m/t=10$, $\theta=\pi/4$)

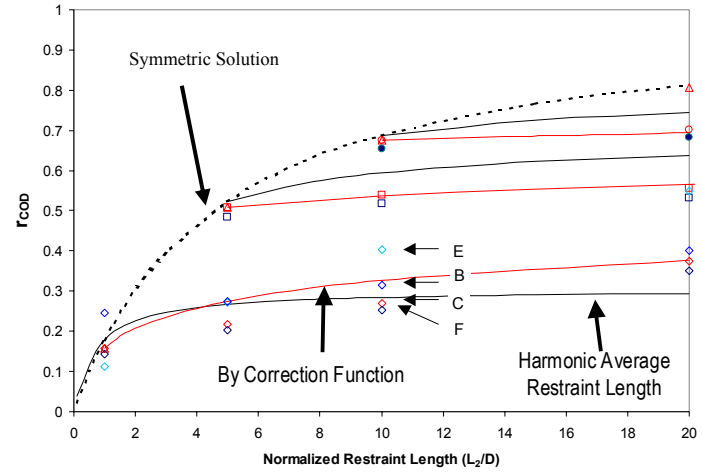

Figure D.20 Verification of analytical expression for asymmetric restraint cases ($R_m/t=10$, $\theta=\pi/2$)

D.4 Pipe Stiffness

In the previous sections of this appendix, the expression for the normalizing factor r_{COD} related the crack-opening displacement (COD) of restrained pipes to the COD for unrestrained pipes. The variable r_{COD} is expressed in terms of the restraint length to mean diameter ratio, L_R/D_m. Although conceptually easy to understand, the restraint length is a difficult parameter to determine directly. Restraint can occur in many forms, from pipe bends and curves to hinges and supports, all of which affect the restraint length in an unpredictable manner. Therefore, in order for the equations for the reduced COD to be practical, it is necessary to express L_R/D_m in terms of an alternate variable. Pipe stiffness is a parameter that is readily calculable in practice using a finite element analysis model. For the crack opening displacement problem, pipe stiffness k can be defined as the "relative moment for a unit kink angle" (see Figure D.21), or

$$k = M / \theta , \qquad (D.17)$$

where

M = applied moment, and
θ = the bending angle.

By deriving expressions relating the pipe stiffness to the normalized restraint length L_R/D_m, it is possible to utilize the r_{COD} equations in practical situations.

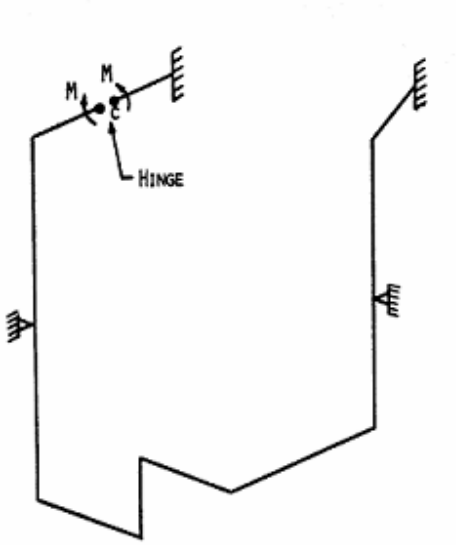

Figure D.21 Moment about a hinge; bends and various supports affect the restraint lengths of the pipe about the hinge

D.4.1 Case Matrix

The following work is based on a matrix of cases very similar to the ones presented in the previous sections. For the symmetric analysis, the cases consisted of the matrix of Table D.1, as well as the matrix of Table D.3 (below). Note that the additional cases in Table D.3 were not a part of the Round-Robin FE analyses or used to derive the r_{COD} equations. Rather, they were additional cases used in the derivation of the equations in the following sections, and allowed for a much more comprehensive analysis of the concept of pipe stiffness.

The r_{COD} equations for asymmetric restraint cover a much narrower range of data. Specifically, the expression for the reference restraint length (Eq. D.16) is valid only when $R_m/t = 10$ and $1/8 < \theta/\pi < ½$. The case matrix of Table D.2 adequately covers this limited range, and therefore only the matrix of Table D.2 is used to develop the L_R/D_m versus k relationship for the case of asymmetric restraint.

D.4.2 The ANSYS Model

In order to determine the pipe stiffness associated with various restraint lengths, a beam-type finite element model of a pipe was created with the ANSYS finite element program. The model elements were the same as the "pipe" elements that would be used in a plant piping stress analysis. The pipe was restrained at either end, and a hinge was created about which a moment could be applied (see Figure D.22).

In order to use the hinge model shown in Figure D.22, one has to settle on precisely how the analysis is to be performed. The hinge concept is quite simple, but there are subtle details that need to be defined. It was determined that the most rational way to proceed is to consider a separate "left" and "right" stiffness corresponding to L_1 and L_2 by finding the stiffness for the respective side assuming that the rotation for the opposite side is fixed at zero. This was, by no means, the only way to perform the stiffness analysis, but it had the desirable effect of more or less uncoupling the "left" and "right" rotations.

Following this idea, the steps for calculating the hinge stiffnesses for a pipe are as follows:

1. Put a hinge at the point of interest with the axis of rotation in the correct 3D orientation. Typically, this is most easily done using local coordinates at the point of interest.
2. Fix the rotation of the "left" side of the hinge at zero in the local coordinate system.
3. Apply a unit moment to the "right" side of the hinge and recover the rotation. The moment M and the recovered rotation θ_2 must both be in the local coordinate system.
4. Repeat steps 2 to 4 replacing "left" with "right" and vice versa in order to determine θ_1.

Table D.3 Additional Symmetric Cases used in Pipe Stiffness Analysis

	OD (mm)	R_m/t	Half Crack Length (radians)			Restraint Length (normalized to the *outer diameter*) L/OD			
Case 4.a	526.13	15	π/8	π/4	π/2	1	5	10	20
Case 4.b	465.23	15	π/8	π/4	π/2	1	5	10	20
Case 4.c	75.00	15	π/8	π/4	π/2	1	5	10	20
Case 5.a	465.23	5	π/8	π/4	π/2	1	5	10	20
Case 5.b	465.23	20	π/8	π/4	π/2	1	5	10	20
Case 5.c	465.23	40	π/8	π/4	π/2	1	5	10	20
Case 6.a	200.00	10	π/8	π/4	π/2	1	5	10	20
Case 6.b	500.00	10	π/8	π/4	π/2	1	5	10	20
Case 6.c	600.00	10	π/8	π/4	π/2	1	5	10	20
Case 7.a	200.00	15	π/8	π/4	π/2	1	5	10	20
Case 7.b	500.00	15	π/8	π/4	π/2	1	5	10	20
Case 7.c	600.00	15	π/8	π/4	π/2	1	5	10	20
Case 8.a	711.20	10	π/8	π/4	π/2	1	5	10	20
Case 8.b	711.20	15	π/8	π/4	π/2	1	5	10	20
Case 8.c	711.20	25	π/8	π/4	π/2	1	5	10	20
Case 9.a	465.23	10	π/8	π/4	π/2	1	5	10	20
Case 9.b	465.23	15	π/8	π/4	π/2	1	5	10	20
Case 9.c	465.23	25	π/8	π/4	π/2	1	5	10	20

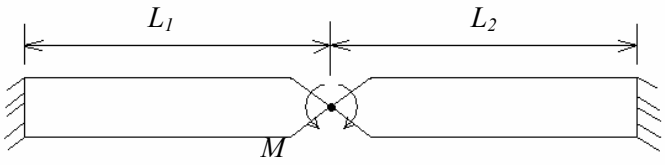

Figure D.22 Schematic of ANSYS pipe model used to determine stiffness values given various restraint lengths

5. For a case of symmetric restraint, divide the moment M by the difference of the rotations $|\theta_1| - |\theta_2|$ in order to determine $k = | M/(|\theta_1| - |\theta_2|)|$. For cases of asymmetric restraint, determine separate stiffness values for the two sides of the hinge as follows: $k_1 = | M/\theta_1 |$ and $k_2 = | M/\theta_2 |$.

The procedure outlined above can be applied as easily to a 3D pipe system with a crack in any orientation as it can be to the simple 2D model shown in Figure D.22.

D.4.3 Pipe Stiffness in Cases of Symmetric Restraint

After running the ANSYS model to determine the stiffnesses for the cases in Tables D.1 and D.3, plots of the restraint length in terms of pipe stiffness were generated for each case. From the plot of Case 1.a (see Figure D.23), it is evident that L_R/D_m and k are related by a power law function. Each case produced a similar plot, with a different constant in front of the power function. It was speculated that this constant was in some way related to the second moment of area of the pipe, I. Plotting the I of a pipe

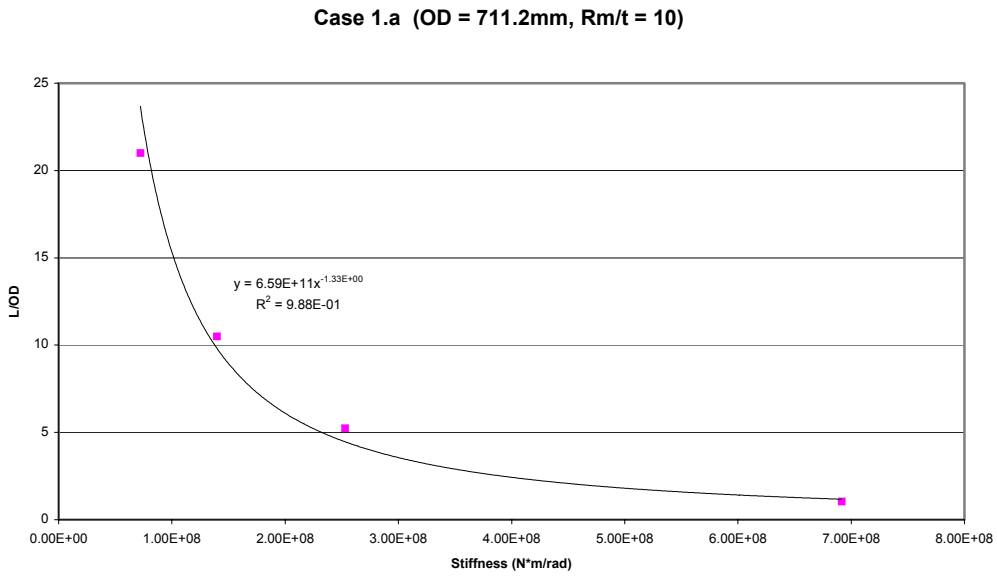

Figure D.23 Plot of restraint length in terms of stiffness for symmetric Case 1; k and L_R/D_m are related by a power function multiplied by a constant

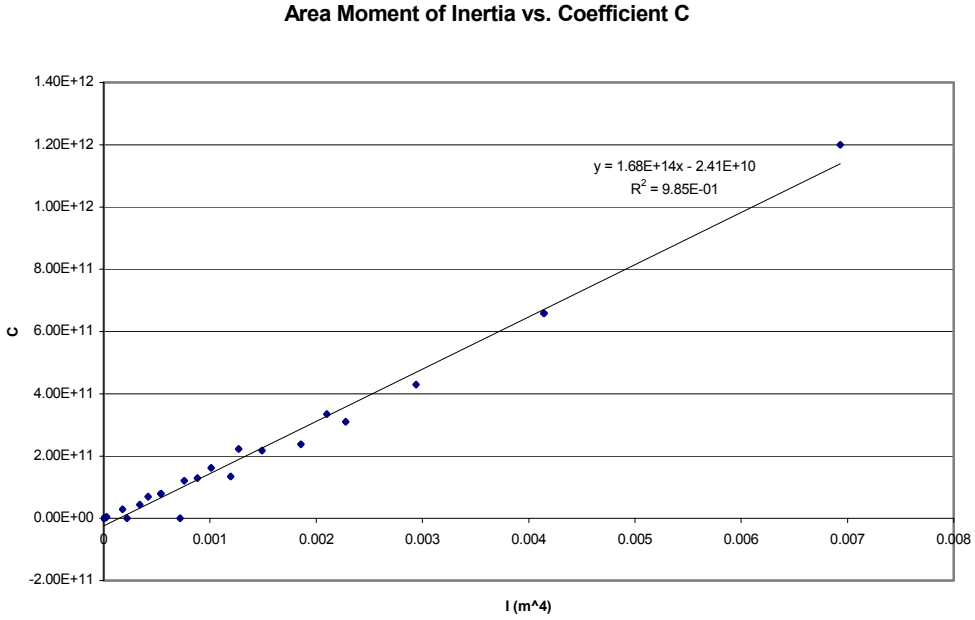

Figure D.24 Plot of constant C in terms of second moment of area I for all symmetric cases (The second moment of area is linearly related to the constant C)

against the required constant, it was clear that the constant is related linearly to I (see Figure D.24).

For cases of symmetric restraint, the following equation was developed relating pipe stiffness and the normalized restraint length,

$$L_R / D_m = Ck^{-1.33}, \qquad (D.18)$$

where L_R/D_m is the normalized restraint length and k is the pipe stiffness in N·m/rad. C is a constant obtained from the following equation

$$C = (1.68 \cdot 10^{14})I - 2.41 \cdot 10^{10} \qquad (D.19)$$

where I is the second moment of area of the pipe cross section (m^4), equivalent to

$$I = \frac{\pi}{64}(D_0^4 - D_i^4). \qquad (D.20)$$

The beam-type finite element analyses shows that the behavior of pipes with an I less than 10^{-4} m^4 does not fit the form of Equations D.18 and D.19 when subjected to a bending moment, and therefore must be related in a different manner to the restraint length. For instance, Cases 1.c and 4.c, where the outer diameters are 0.1143 m (4.5 inches) and 0.075 m (3.0 inches), respectively, and the thicknesses are both less that 10 mm (0.4 inches), show significant deviation from the expected behavior. Consequently, Equations D.18 through D.20 are accurate only when the second moment of area is greater than or equal to 10^{-4} m^4 (240 $inch^4$).

The plot in Figure D.25 shows the comparison between the normalizing factor r_{COD} when calculated using the parametric values of L_R/D_m and the stiffness-based values of L_R/D_m resulting from use of the above equations. Error appears to increase significantly as the second moment of area of the pipe cross-section approaches the range limit of 10^{-4} m^4 (240 $inch^4$).

D.4.4 Pipe Stiffness in Cases of Asymmetric Restraint

In the case of asymmetric restraint, the equations relating the pipe stiffness to the restraint length have the same form as in symmetric restraint with a slightly different scale. The two restraint lengths can be calculated using the equations

$$L_{R1} / D_m = C_1 k_1^{-1.11} \text{ and } L_{R2} / D_m = C_2 k_2^{-1.12}. \qquad (D.21)$$

Again, C_1 and C_2 are constants, and are dependent on the pipe's second moment of area as follows:

$$C_1 = (3.19 \cdot 10^{12})I + 2.07 \cdot 10^{8}$$
$$C_2 = (1.04 \cdot 10^{13})I + 6.92 \cdot 10^{8} \qquad (D.22)$$

In this case, k_1 and k_2 represent the stiffness of the pipe corresponding to the rotation of L_1 and L_2, respectively. As in the symmetric cases, the differences between parametric and stiffness-based L_R/D_m values when $I < 10^{-4}$ m^4 (240 $inch^4$) are significant, and the equations should not be utilized in this range.

Figures D.26 and D.27 (below) illustrate the power relationship between L_{R1}/D_m and L_{R2}/D_m and k, and the comparison between r_{COD} values, respectively.

D.5 Application of Equations

After developing the equations for r_{COD} in terms of pipe stiffness, it was important to apply them to some plant piping cases to see what effect the revised COD values have on leak rates for actual plant piping applications. This gives the user an idea of the importance of the pressure-induced bending effect in the calculation of crack-opening displacement values for a plant LBB application.

A finite element model of a 3-loop Westinghouse-style PWR nuclear power plant was developed, and hinges were placed at eighteen critical locations per the procedure given in Section D.4.2. Figures D.28 through D.31 show the 18 locations, all of which were at

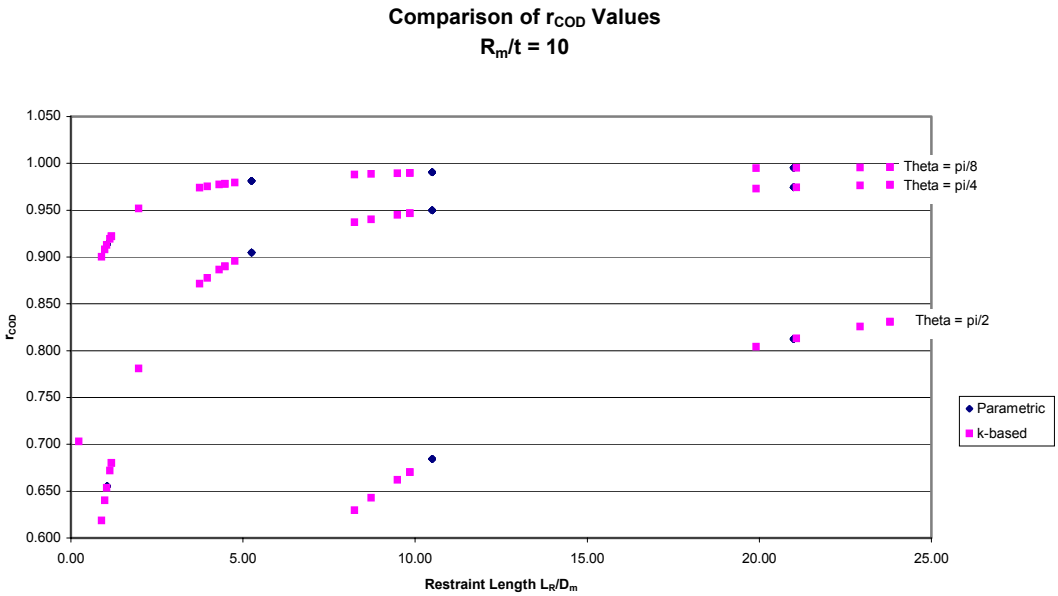

Figure D.25 Comparison of normalizing factors for parametric and stiffness-based L_R/D_m values in cases of symmetric restraint

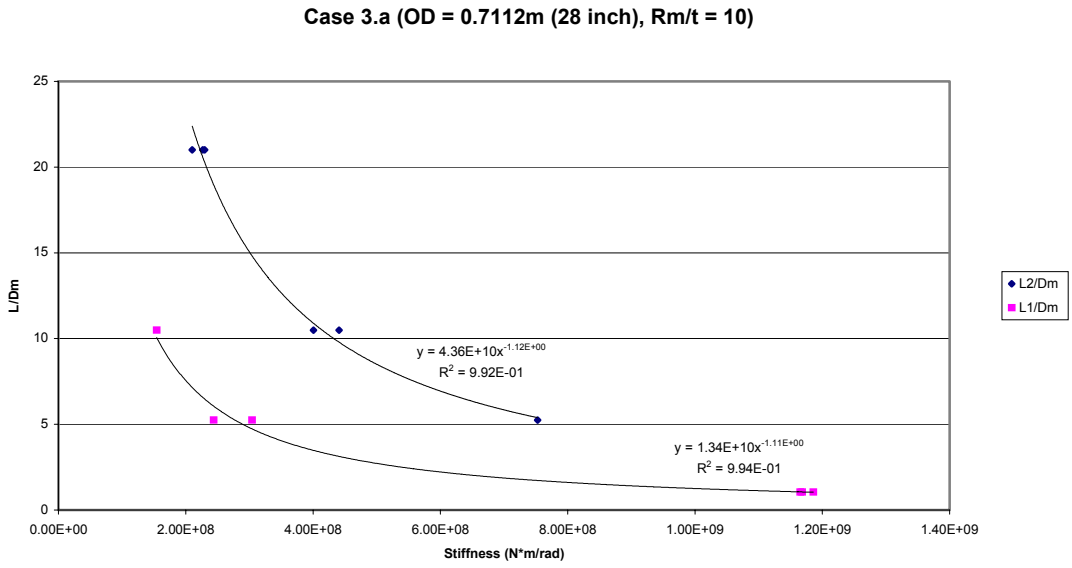

Figure D.26 Plot of restraint length in terms of stiffness for asymmetric Case 1.a

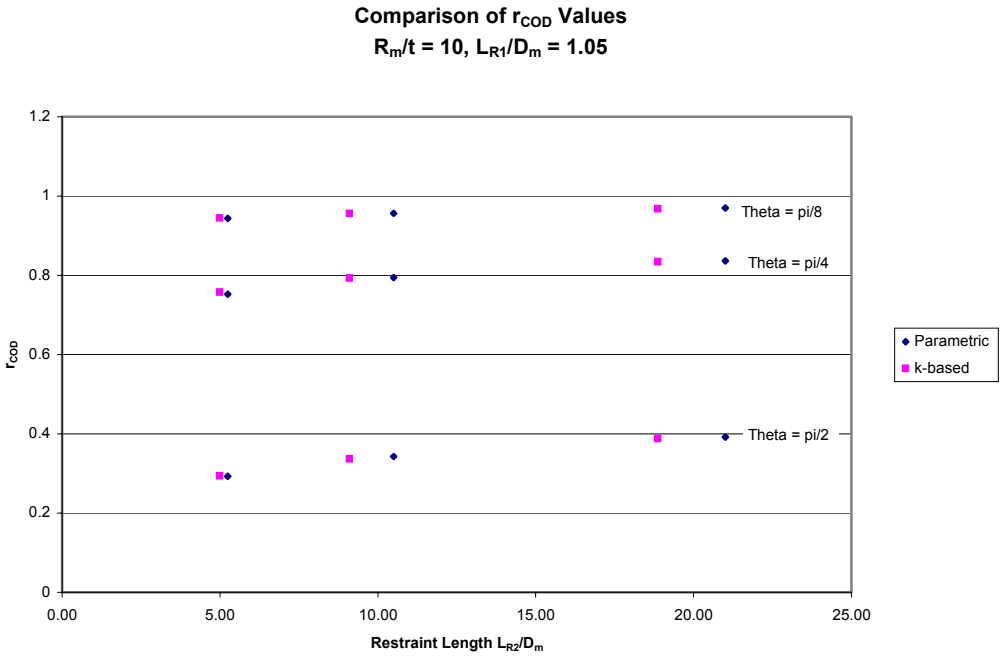

Figure D.27 Comparison of normalizing factor between parametric and stiffness-based values of L_R/D_m for asymmetric restraint

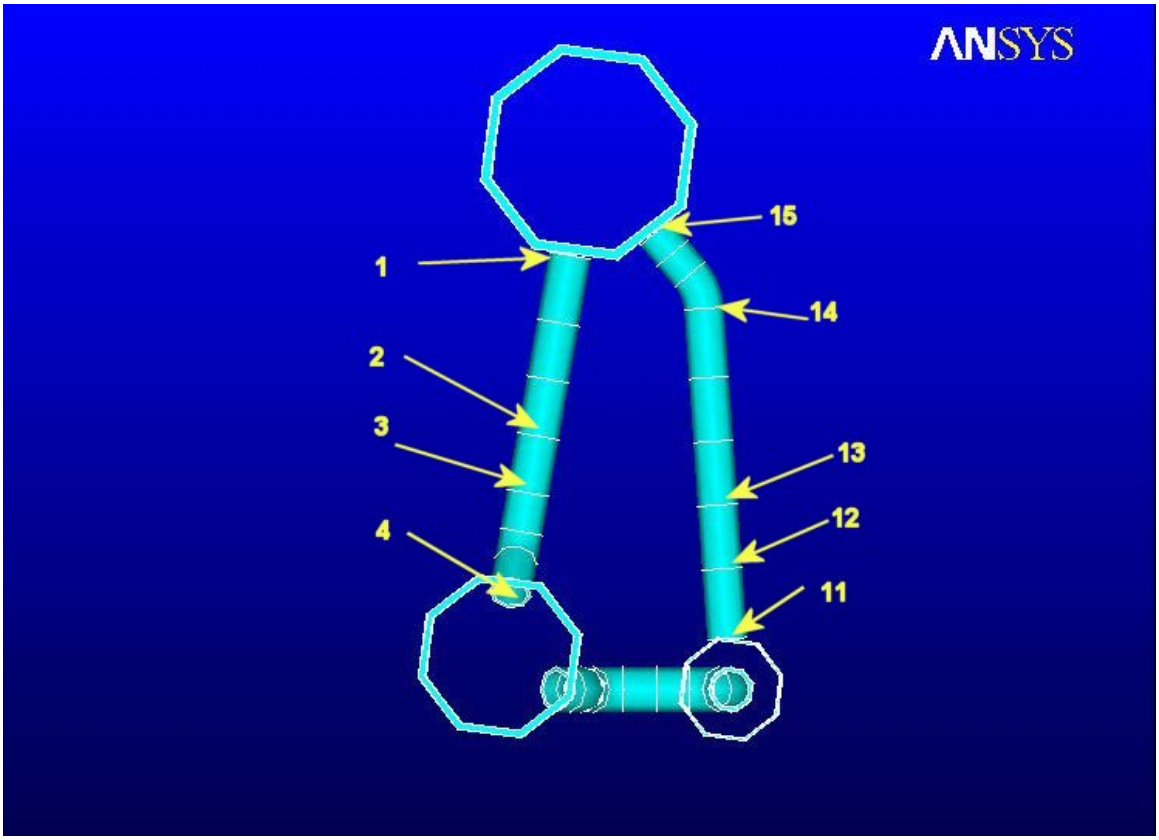

Figure D.28 Critical flaw locations in the hot and cold legs

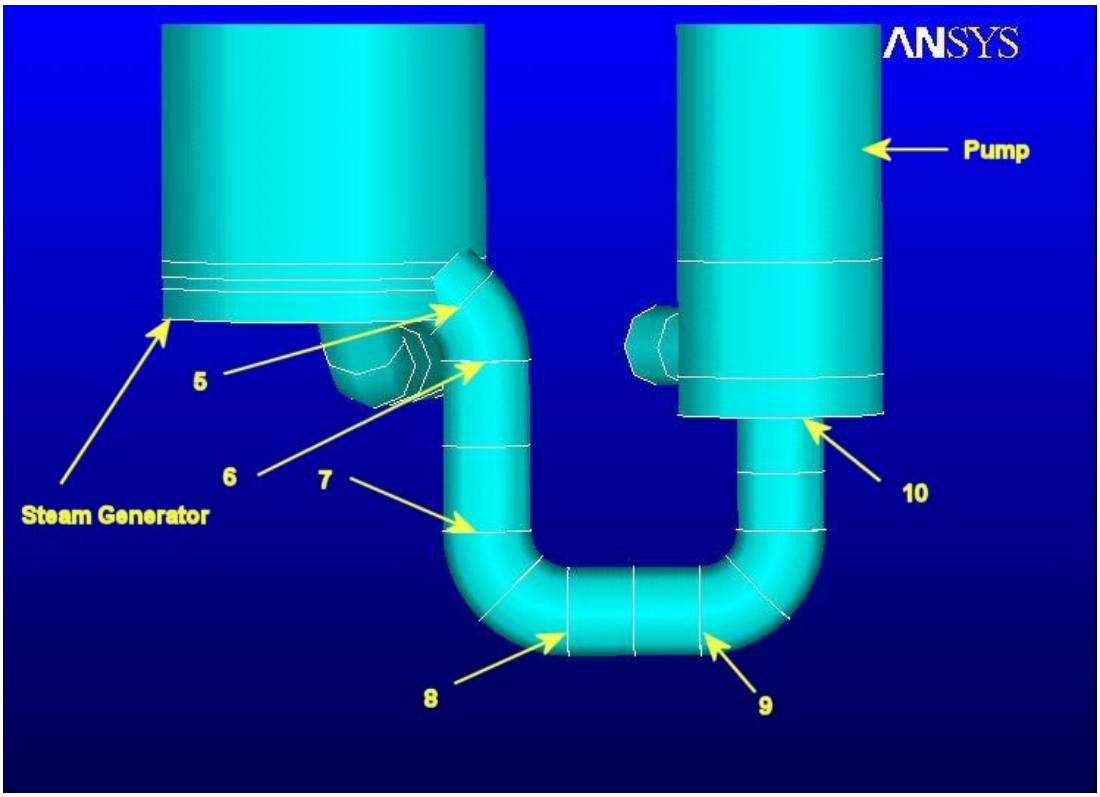

Figure D.29 Critical flaw locations in the crossover leg

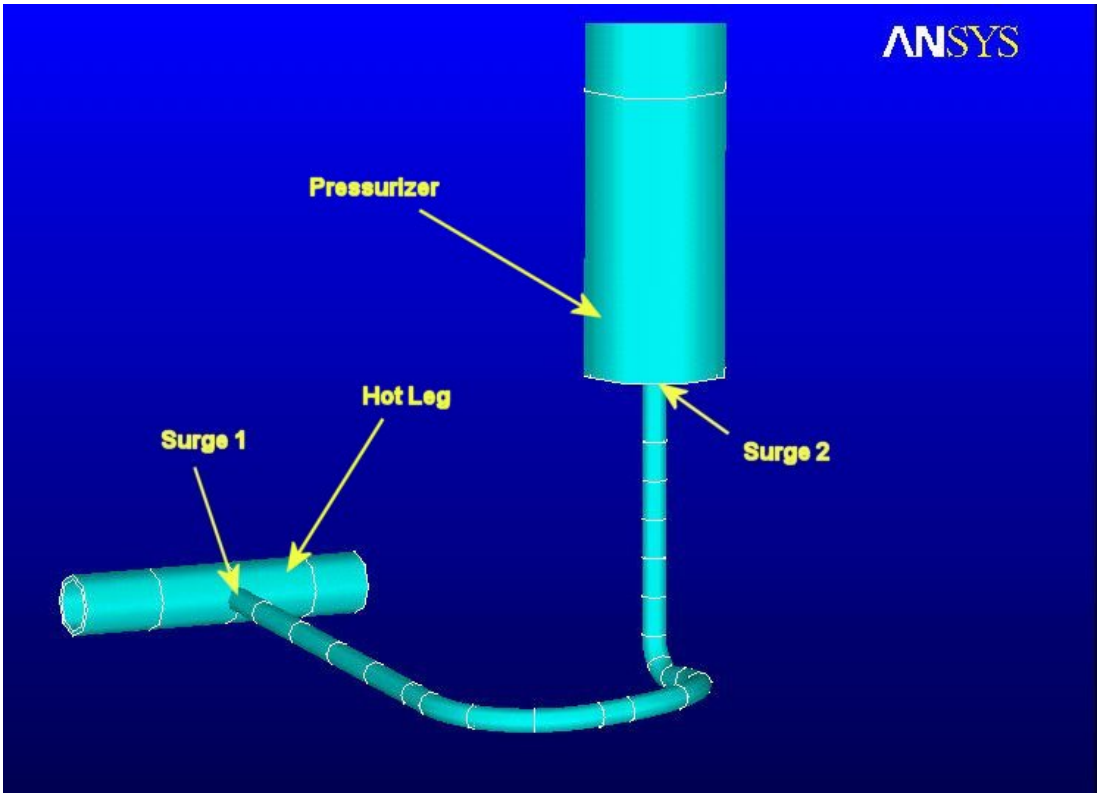

Figure D.30 Critical flaw locations in the surge line

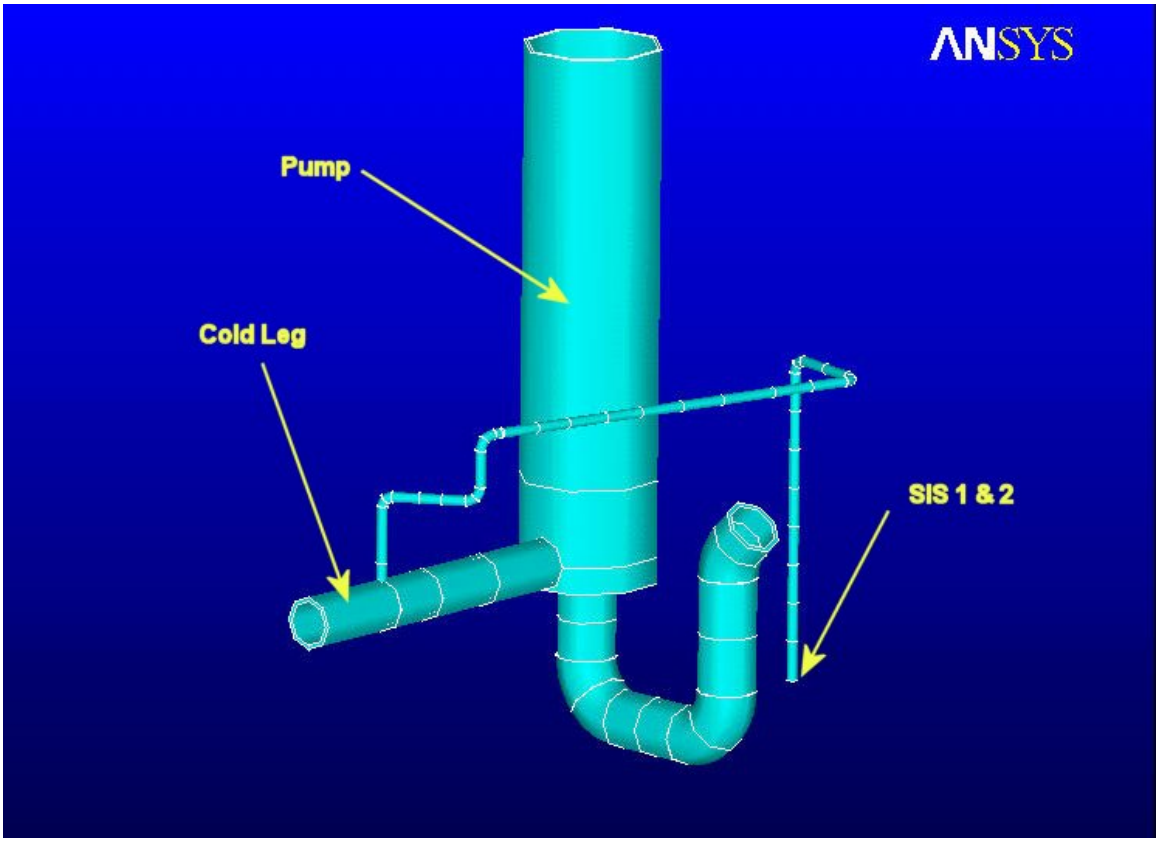

Figure D.31 Critical flaw locations in the safety injection system

Table D.4 Dimensional and loading conditions for 18 critical locations considered in sample plant piping system test cases

Case Data

	Location	R_i (in)	t_{wall} (in)	OD (in)	M_b (in*lb)	F_x	Temp (°F)	Pressure (psi)
Primary System	1	14.6	2.37	33.94	12591000	1504000	610	2235
	2	14.6	2.37	33.94	4491000	1504000	610	2235
	3	14.6	2.37	33.94	12435000	1505000	610	2235
	4	15.6	3.15	37.5	15098000	1633000	610	2235
	5	15.6	3.15	37.5	13805000	1597000	542	2200
	6	15.6	2.52	36.24	12632000	1564000	542	2200
	7	15.6	2.52	36.24	13047000	1557000	542	2200
	8	15.6	2.52	36.24	6425000	1684000	542	2200
	9	15.6	2.52	36.24	1086000	1684000	542	2200
	10	15.6	3.18	37.56	5639000	1844000	542	2200
	11	13.85	2.25	32.2	1689000	1388000	542	2300
	12	13.85	2.25	32.2	2398000	1389000	542	2300
	13	13.85	2.25	32.2	2339000	1389000	542	2300
	14	13.85	2.25	32.2	2418000	1386000	542	2300
	15	13.85	2.36	32.42	2742000	1342000	542	2300
Surge Line	1	5.754	1.246	14	1545839	221161	653	2327
	2	5.754	1.246	14	1766184	234511	617	2327
SIS	1	2.5945	0.718	6.625	136539	-1083	105	2327

high stress points or at field welds. Table D.4 provides the pertinent dimensional and loading conditions for these particular locations. Because the angular position of the postulated leaking flaw was not known, the rotation was calculated at 15-degree intervals around the pipe circumference at each location. The largest rotation was assumed to correspond with the orientation of the flaw, and this rotation was used in subsequent calculations. After calculating the pipe stiffness, Equations D.18 and D.21 were used to determine the restraint lengths, and Equations D.3 and D.14 were used to calculate the values of r_{COD}. Note, Equations D.3 and D.18 are for the symmetric restraint case and Equations D.14 and D.21 are for the asymmetric restraint cases. While each of the cases were asymmetric, the equations for the asymmetric case were developed for a specific R/t ratio (R/t = 10). The R/t ratio for each of these cases was close to 5, typical of PWR piping. Thus, the symmetric case, which is was developed for a wider range of R/t ratios, was considered as well. Further note that preliminary analyses to date suggest that the effect of using the R/t solutions for the asymmetric case developed to date for pipes with R/t ratios less than 10 (typical of PWR piping) would result in a longer crack length for a given leak rate detection limit capability in an LBB analysis, i.e., a conservative assessment of crack length. Thus, the use of the asymmetric solution for these sample applications should provide an upper-bound illustration of the impact of this effect. However, if a more generalized asymmetric solution is desired, then a curve fit equation through multiple finite element analyses is needed for different R/t ratio cases.

Once the normalizing factors were obtained, it was necessary to calculate the COD of the unrestrained pipe. The SQUIRT program was utilized in this endeavor. The crack morphology parameters for an IGSCC crack were assumed. Once calculated, COD_{unres} was multiplied by r_{COD} to determine COD_{res}. On first glance, (see Table D.5), the values appear to be so close together that any difference would be insignificant, i.e., less than 10 percent.

Table D.5 Comparison between restrained and unrestrained COD values

Pipe System		SQUIRT Calcs.					Symm. Rest. COD	% diff. respect to unrest. COD	Asymm. Rest. COD	% diff. respect to unrest. COD
				Normalized Restraint Lengths						
(Leak Rate)	Location	Unrest. COD	Crack Length	Symmetric	Asymmetric					
				L/D_m	L_1/D_m	L_2/D_m				
		(in)	inch				inch		(in)	inch
Primary	1	0.0217	13.33	4.1	0.1	17.9	0.0212	2.5%	0.0217	0.0%
(5 gpm)	2	0.0178	16.3	11.2	5.8	23.8	0.0175	1.5%	0.0175	2.0%
	3	0.0216	13.38	11.6	6.4	22.9	0.0214	0.9%	0.0214	1.2%
	4	0.0203	16.48	15.3	0.3	58.1	0.0201	0.9%	0.0203	0.0%
	5	0.0147	14.31	11.4	0.8	42.9	0.0146	0.9%	0.0145	1.6%
	6	0.0154	12.22	16.8	6.5	40.2	0.0154	0.5%	0.0153	0.7%
	7	0.0156	12.13	29.0	6.9	73.4	0.0156	0.3%	0.0155	0.5%
	8	0.0136	13.97	20.9	10.0	42.0	0.0135	0.5%	0.0135	0.7%
	9	0.0088	21.8	18.3	9.9	34.8	0.0087	1.6%	0.0086	2.2%
	10	0.0126	16.75	38.5	1.0	125.3	0.0126	0.4%	0.0126	0.0%
	11	0.0112	15.85	4.8	1.0	16.5	0.0107	3.7%	0.0104	6.6%
	12	0.0124	14.17	7.1	3.6	16.2	0.0121	1.9%	0.0121	2.5%
	13	0.0123	14.31	9.1	5.6	16.8	0.0121	1.5%	0.0121	1.9%
	14	0.0125	14.17	9.9	6.1	17.8	0.0123	1.4%	0.0123	1.7%
	15	0.0126	14.34	5.6	0.1	22.7	0.0123	2.4%	0.0126	0.0%
Surge	1	0.0257	10.09	22.6	3.0	60.9	0.0252	1.9%	0.0241	6.1%
(5 gpm)	2	0.0233	9	7.9	0.1	29.0	0.0223	4.0%	0.0231	0.7%
Surge	1	0.0447	11.79	22.6	3.0	60.9	0.0435	2.8%	0.0405	9.5%
(10 gpm)	2	0.0392	10.85	7.9	0.1	29.0	0.0367	6.3%	0.0357	8.8%

After studying the cases listed above, it is natural to wonder when, if ever, the normalizing factor would have a significant effect on the COD. From the previous plots, it can be seen that as the crack angle increases, the difference between the unrestrained and restrained COD values increases. Referring back to Figures D.25 and D.27, it is clear that r_{COD} values for a half-crack angle of $\pi/2$ are much smaller than those for a half-crack angle of $\pi/8$. Thus, one condition that must be satisfied in order for the effect of restraint of pressure induced bending to be significant is the crack angle (2**2**) must be relatively large. For leak-before-break analyses, this is most likely for smaller diameter pipe. However, as alluded to earlier, the L/D analysis developed as part of this program is presently limited to pipes with moments of inertia greater than 10^{-4} m^4 (240 $inch^4$). It can be readily shown that the pipe diameter must be at least 10-inch, regardless of pipe schedule, for this condition to be satisfied[1]. While the pipe schedule for 10-inch diameter pipe must be at least schedule 80.[2] For 10-inch diameter Schedule 160 pipe, the leakage crack size from a SQUIRT4 analysis, assuming a relatively low operating stress[3] of $0.4S_m$ ($P_m + P_b$) is only about 40 percent of the pipe circumference for a (1.0 gpm) leakage detection system and assuming crack morphology parameters for an IGSCC crack[4]. If the normal operating loads are higher, or the leakage

[1] The moment of inertia for a 8-inch diameter schedule 160 pipe is 7×10^{-5} m^4 (166 $inch^4$).
[2] The moment of inertia for a 10-inch diameter schedule 80 pipe is 10^{-4} m^4 (245 $inch^4$).
[3] The lower the operating stress, the longer the leakage crack size from an LBB perspective.
[4] The relatively coarse leakage detection limit (1.0 gpm versus 0.5 gpm) and relatively rough crack surface of an IGSCC crack versus a fatigue crack both tend to result in longer leakage flaw sizes.

detection system is better (0.5 versus 1.0 gpm), or if the crack surface is not so torturous (fatigue versus IGSCC), then the leakage crack size will be even shorter.

The other condition, besides large crack angle, that must be satisfied in order for the effect of restraint of pressure induced bending to be significant is that the L/D parameter must be small, see Figure D.16. This is more likely to occur for the stiffer (i.e., larger diameter) pipe. Thus, the two conditions that must both be satisfied for this effect to be significant are to an extent mutually exclusive, such that for most practical applications, one can probably ignore this effect. The only potentially significant applications where one may want to consider this effect is very small diameter pipe, less than 6- or 8-inch diameter. However, as noted previously, for these small diameter piping systems, the L/D analysis proposed herein that is based on rotational stiffness is not valid, or cases where one is considering a postulated crack at a location where the piping system attaches directly to a vessel, e.g., where the surge line connects to the pressurizer. However, that case was analyzed as one of the 18 locations already considered (Surge 2) and the effect on the COD was shown to be minimal.

D.6 Conclusion

The center crack-opening displacement at the mid-thickness of a through-wall circumferential crack in a straight pipe under end-restraint condition can be evaluated using the crack-opening displacement of the corresponding unrestrained pipe and the normalizing factor derived in this program.

$$COD_{res} = r_{COD} \cdot COD_{unres} \qquad (D.23)$$

Analytical expressions for the normalizing factor, r_{COD}, have been derived. It was found that Miura's solution of Equation D.4, combined with the revised $I_b(\theta, R_m/t)$ function of Equation D.7, can be used to evaluate r_{COD} for a symmetrically restrained pipe. A correction function (Equation D.14) has been proposed to relate the r_{COD} for an asymmetrically restrained pipe to that of the corresponding symmetrically restrained pipe. The validity of these analytical expressions has been examined using the COD results from the Round-Robin FE analyses conducted previously in the BINP program, see Appendix I.

In order to apply these equations in a practical manner, it was necessary to express the restraint length (L/D) in terms of another variable which was more easily calculable. Equations were developed relating the restraint length to the pipe stiffness. The results from these equations match closely with the previous L_R/D_m parametric equations, thus validating their accuracy. The expressions for the normalizing factor and the restraint length in terms of pipe stiffness are semi-empirical in nature, and should be used within the range which the expressions were derived.

In terms of practical application, it appears that effect of restraint of pressure-induced bending is negligible in PWR primary piping. Unless the tolerable leak rate is so large that the normal operating crack approaches 180 degrees, the effect of restraint of pressure induced bending on COD is not a factor.

D.7 References

D.1 Ghadiali, N., Rahman, S., Choi, Y. H. and Wilkowski, G., "Deterministic and Probabilistic Evaluations for Uncertainty in Pipe Fracture Parameters in Leak-Before-Break and In-Service Flaw Evaluations," U.S. Nuclear Regulatory Commission, NUREG/CR-6443, 1996.

D.2 Rahman, S., Ghadiali, N., Paul, D., and Wilkowski, G., "Probabilistic Pipe Fracture Evaluations for Leak-Rate Detection Applications," NUREG/CR-6004, April 1995.

D.3 Rahman, S., Brust, F., Ghadiali, N., Choi, Y. H., Krishnaswamy, P., Moberg, F., Brickstad, B., and Wilkowski, G., "Refinement and Evaluation of Crack-Opening-Area Analyses Circumferential Through-Wall Cracks in Pipes for Circumferential Through-Wall Cracks in Pipes," U.S. Nuclear Regulatory Commission, NUREG/CR-6300, 1995.

D.4 Wilkowski, G., Feng, Z., Miura, N, Choi, J.B., Ghadiali, N., Choi, Y.H., Santos, C., Brust, F. and Scott, P., "Round-Robin Finite Element Analysis of Crack-Opening Displacements in Axially Loaded Piping Systems for Leak-Before-Break Applications – Effect of Pipe System Restraint on Pressure-Induced Bending," BINP Program Report.

D.5 Miura, N. "Evaluation of Crack Opening Behaviors for Cracked Pipes – Effect of Restraint on Crack Opening," *Proc. ASME PVP Conf.* PVP-Vol. 423, 2001, pp. 135-143.

D.6 Klecker, R., Brust, F.W. and Wilkowski, G., "NRC Leak-Before-Break (LBB.NRC) Analysis Method for Circumferentially Through-Wall-Cracked Pipes under Axial Plus Bending Loads," NUREG/CR-4572, 1986.